Lattice kinetic simulation of nonisothermal magnetohydrodynamics

Dipankar Chatterjee[1,*] and Sakir Amiroudine[2]
[1]*Simulation & Modeling Laboratory, Central Mechanical Engineering Research Institute (Council of Scientific & Industrial Research), Durgapur-713209, India*
[2]*Laboratoire TREFLE UMR CNRS 8508, Esplanade des Arts et Métiers, 33405 Talence Cedex, France*
(Received 5 June 2009; revised manuscript received 16 March 2010; published 16 June 2010)

In this paper, a lattice kinetic algorithm is presented to simulate nonisothermal magnetohydrodynamics in the low-Mach number incompressible limit. The flow and thermal fields are described by two separate distribution functions through respective scalar kinetic equations and the magnetic field is governed by a vector distribution function through a vector kinetic equation. The distribution functions are only coupled via the macroscopic density, momentum, magnetic field, and temperature computed at the lattice points. The novelty of the work is the computation of the thermal field in conjunction with the hydromagnetic fields in the lattice Boltzmann framework. A 9-bit two-dimensional (2D) lattice scheme is used for the numerical computation of the hydrodynamic and thermal fields, whereas the magnetic field is simulated in a 5-bit 2D lattice. Simulation of Hartmann flow in a channel provides excellent agreement with corresponding analytical results.

DOI: 10.1103/PhysRevE.81.066703 PACS number(s): 47.11.−j, 51.10.+y, 47.35.Tv, 47.65.−d

I. INTRODUCTION

The multiscale mesoscopic lattice Boltzmann (LB) methods have already been proven to be an efficient and inexpensive tool to simulate complex thermofluidic phenomena. They have been successfully utilized as an alternative to the conventional computational fluid dynamics (CFD) methods for incompressible low-Reynolds number flows in topologically complex geometries, including porous media and particulate suspension multiphase flows. A distinct advantage of this approach is that the method is fundamentally based on microscopic particle models and mesoscopic kinetic equations, so that the microscale and mesoscale physics can be elegantly bonded together. Another important advantage, in comparison to the classical continuum based formulation, is that it does not require an immediate explicit calculation of fluid pressure, leading to time-efficient computations. Furthermore, LB models are inherently parallelizable, since the nonlocalities can be restricted to nearest-neighbor interactions alone, and the only additional computations involved are equivalent to that of a mere streaming step, which renders them suitable to address multiscale thermofluidic processes over large-scale computational domains [1].

Magnetohydrodynamics (MHD) has been a subject of intense research for long time due to its overwhelming importance in numerous fields ranging from several natural phenomena such as geophysics, astrophysics to many engineering applications such as plasma confinement, liquid-metal cooling of nuclear reactors, electromagnetic casting and so on. Significant effort has so-far been directed toward LB modeling of two-dimensional (2D) MHD flows [2–8] to describe the isothermal hydro-magnetic interactions. Most of them utilize a tensor distribution function f_a^σ (with $\sigma = 1, \ldots, S$, where S is the total number of components in the fluid system and $a = 0, \ldots, b$, where b is the number of the nearest-neighboring sites) whose moments produce all the pertinent macroscopic quantities. However, this approach requires the introduction of a second base vector for the discrete particle velocities [5]. Although subsequent efforts have also been devoted to optimize the approach by reducing the complexity of the system, this formulation adds significant burden on computation and consequently the extension to three-dimensional (3D) geometry becomes reasonably cumbersome [9]. Dellar [10] proposed a better way to reduce the computer memory by representing the magnetic field through a vector valued distribution function, which obeys a kinetic BGK (Bhatnagar-Gross-Krook)-type evolution equation. The associated hydrodynamics is simulated by a typical BGK LB model and the Lorentz force is introduced into the MHD formulation by a heuristic extension of the equilibrium distribution function (EDF). An important advantage of this formulation is that the kinetic viscosity can be independently adjusted from the magnetic resistivity. This model is extended to 3D in a straightforward manner by Breyiannis and Valougeorgis [11] where the Lorentz force is introduced as a pointwise force through a systematic and conventional approach based on the *a priori* derivation of the BGK equation with an external acceleration term. It is to be emphasized once again that all of the abovementioned LB models assume an isothermal MHD flow and no serious attempt has so far been made to compute the nonisothermal MHD flow in the LB framework. However, recently, Niu *et al.* [12] developed a LB model for ferrohydrodynamics to simulate temperature-sensitive ferrofluids. The magnetic field is modeled in [12] using a scalar magnetic potential and the model assumes the collinear situation of magnetization and magnetic intensity in a narrow range of magnetic field strength and temperature.

We aim here to propose a lattice kinetic simulation strategy for nonisothermal MHD flows in an incompressible limit (which is the limit of small Mach number, $\mathrm{Ma} \to 0$). The model originates from a conventional single fluid hydrodynamic description based on a scalar kinetic equation and subjected to an external electromagnetic (Lorentz) force. The thermal field is obtained by another scalar kinetic equation following the passive scalar approach of He *et al.* [13] and

*Corresponding author. FAX: +91-343-2548204; d_chatterjee@cmeri.res.in

incorporating the Joule heating effect and the magnetic induction is modeled by a vector kinetic equation following Dellar [10]. The Lorentz force and the Joule heating source term are introduced in the respective kinetic equations by the most formal technique following the extended Boltzmann equation [13]. Since three separate kinetic equations are used to simulate the fluid momentum, thermal and magnetic fields, the kinetic viscosity, thermal diffusivity, and magnetic resistivity can be independently adjusted which makes the model suitable for variable Prandtl (thermal as well as magnetic) number MHD flows.

The rest of the paper is organized as follows: Section II is devoted to the formulation of the scheme. We briefly present the macroscopic conservation equations and subsequently the evolution of hydrodynamic, magnetic and thermal LB schemes along with the pertinent macroscopic quantities. In Sec. III, numerical simulations are performed for a nonisothermal Hartmann flow in a 2D channel and results are compared with the analytical results. The final section (Sec. IV) summarizes the present findings.

II. MODEL FORMULATION

A. Macroscopic conservation equations

We start with the macrodynamical behavior of a classical MHD system in the low Mach number incompressible limit through the following set of governing equations, which consist of the momentum conservation, magnetic induction and energy conservation, assuming a linear, isotropic conductive media and neglecting any phenomenological cross effects as:

$$\rho(\partial_t \mathbf{u} + \mathbf{u}\cdot\nabla\mathbf{u}) = -\nabla p + \nabla\cdot\boldsymbol{\sigma} + \mathbf{F_L} \tag{1}$$

$$\partial_t \mathbf{B} + \nabla\cdot(\mathbf{uB} - \mathbf{Bu}) = \eta\nabla^2\mathbf{B} \tag{2}$$

$$\rho c_p(\partial_t T + \mathbf{u}\cdot\nabla T) = \nabla\cdot(\kappa_t \nabla T) + \boldsymbol{\sigma}:\nabla\mathbf{u} + q. \tag{3}$$

Here $\mathbf{u}$, p, $\mathbf{B}$, and T denote the macroscopic velocity, pressure, magnetic flux density and temperature, $\boldsymbol{\sigma}=\rho\nu[(\nabla\mathbf{u}+\nabla\mathbf{u}^T)-2/3(\nabla\cdot\mathbf{u})\mathbf{I}]$ is the viscous stress tensor, ρ, ν, η, c_p, and κ_t are the density, kinematic viscosity, magnetic resistivity, specific heat, and thermal conductivity of the electrically conducting fluid, $\mathbf{F_L}=\mathbf{J}\times\mathbf{B}$ is the electromagnetic Lorentz force and $q=\mathbf{J}\cdot\mathbf{J}/\kappa_e$ represents the Joule heating source term, where $\mathbf{J}$ is the electric current density, which is given by the Ampere-Maxwell's law as: $\mathbf{J}=(1/\mu)\nabla\times\mathbf{B}$ with μ and κ_e being the magnetic permeability and electrical conductivity. The electric field has been eliminated in Eq. (3) using Ohm's law as per the usual resistive MHD approximation [10]. Additionally, the solenoidal constraints $\nabla\cdot\mathbf{u}=0$ and $\nabla\cdot\mathbf{B}=0$ are imposed. We neglect here the natural and Marangoni convection, polarization and magnetization, electrostatic induction and electrochemical reactions in the present formulation.

B. Hydrodynamic LB scheme

The lattice kinetic model for the MHD system presented above can be initiated by constructing a scalar kinetic equation directly from the continuous Boltzmann equation with single-relaxation-time BGK approximation through the space and time evolution of a single particle density distribution function (DDF) $f(\mathbf{x},\boldsymbol{\xi},t)$, which monitors the hydrodynamics in presence of an external forcing parameter (F) as:

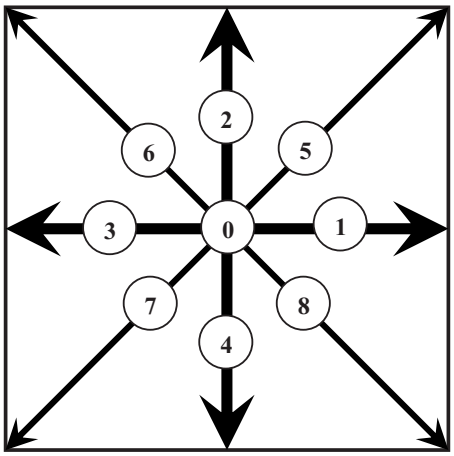

FIG. 1. Two-dimensional nine speed (0–8) (D2Q9) model used for hydrodynamic and thermal simulation. Thick lines with five speeds (0, 1, 2, 3, 4) (D2Q5) represent the lattice used for magnetic field simulation [9].

$$\partial_t f + \boldsymbol{\xi}\cdot\nabla f = -(1/\lambda_f)(f - f^{eq}) + F, \tag{4}$$

where $\boldsymbol{\xi}$ stands for the particle velocity vector, λ_f is the relaxation time and f^{eq} is the local Maxwell-Boltzmann type EDF. Equation (4) is subsequently integrated along its characteristic using the second order trapezoidal rule [13] to yield the evolution equation of the discrete DDF $f_i(\mathbf{x},\boldsymbol{\xi}_i,t)$ $(i\in\{0,N\})$

$$\begin{aligned} f_i(\mathbf{x}+\boldsymbol{\xi}_i\delta t,\boldsymbol{\xi}_i,t+\delta t) - f_i(\mathbf{x},\boldsymbol{\xi}_i,t) &= -\frac{\delta t}{2\lambda_f}[f_i(\mathbf{x}+\boldsymbol{\xi}_i\delta t,\boldsymbol{\xi}_i,t+\delta t) - f_i^{eq}(\mathbf{x}+\boldsymbol{\xi}_i\delta t,\boldsymbol{\xi}_i,t+\delta t)] \\ &\quad - \frac{\delta t}{2\lambda_f}[f_i(\mathbf{x},\boldsymbol{\xi}_i,t) - f_i^{eq}(\mathbf{x},\boldsymbol{\xi}_i,t)] \\ &\quad + \frac{\delta t}{2}F_i(\mathbf{x}+\boldsymbol{\xi}_i\delta t,\boldsymbol{\xi}_i,t+\delta t) + \frac{\delta t}{2}F_i(\mathbf{x},\boldsymbol{\xi}_i,t), \end{aligned} \tag{5}$$

where, the index i stands for the N base vectors of the underlying lattice type and δt denotes the time step. The discrete EDF and the forcing parameter can be constructed as:

$$f_i^{eq} = w_i\rho\left[1 + \frac{(\boldsymbol{\xi}_i\cdot\mathbf{u})}{c_s^2} + \frac{\mathbf{uu}:(\boldsymbol{\xi}_i\boldsymbol{\xi}_i - c_s^2\mathbf{I})}{2c_s^4}\right]$$

and

$$F_i = w_i\left[\frac{\boldsymbol{\xi}_i - \mathbf{u}}{c_s^2} + \frac{(\boldsymbol{\xi}_i\cdot\mathbf{u})}{c_s^4}\boldsymbol{\xi}_i\right]\cdot\mathbf{F_L}.$$

The weights w_i and the discrete velocities $\boldsymbol{\xi}_i$ are so chosen that the mass and momentum are conserved and the symmetry requirements are satisfied. For example, in the 2D nine velocity (D2Q9) $(N=8)$ model (refer to Fig. 1) the weights are given by $w_0=4/9$, $w_i=1/9$ for $i=1-4$, $w_i=1/36$ for

$i=5-8$; the discrete velocities are given by $\boldsymbol{\xi}_0=0$, $\boldsymbol{\xi}_i=\psi_i(\cos\theta_i,\sin\theta_i)$ with $\psi_i=\varphi$, $\theta_i=(i-1)\pi/2$ for $i=1-4$, and $\psi_i=\sqrt{2}\varphi$, $\theta_i=(i-5)\pi/2+\pi/4$ for $i=5-8$ and the sound speed of the model $c_s=\sqrt{RT_0}=\varphi/\sqrt{3}$ with φ and R being the lattice speed and gas constant, respectively. The forcing parameter F_i satisfies the properties: $\Sigma_{i=0}^{N}F_i=0$ and $\Sigma_{i=0}^{N}\boldsymbol{\xi}_i F_i=\mathbf{F_L}$. By using the Chapman-Enskog multiscale expansion and the solvability conditions $\Sigma_{i=0}^{N}f_i^{(n)}=0$, $\Sigma_{i=0}^{N}\boldsymbol{\xi}_i f_i^{(n)}=0$ for $n=1,2,\ldots$, Eq. (5) correctly recovers the Navier-Stokes equations in the incompressible limit setting the kinematic viscosity as $\nu=c_s^2(\lambda_f^*-0.5)\delta t$, where $\lambda_f^*=0.5+(\lambda_f-0.5)/\rho(\mathbf{x},t,T)$ is the modified relaxation time for the nonisothermal flows [14] with $\rho(\mathbf{x},t,T)$ being the local particle density, which is calculated as the local sum over the particle velocity distribution according to $\rho(\mathbf{x},t,T)=\Sigma_{i=0}^{N}f_i(\mathbf{x},t,T)$. The hydrodynamic macroscopic quantities are obtained from $\rho=\Sigma_{i=0}^{N}f_i$ and $\rho\mathbf{u}=\Sigma_{i=0}^{N}\boldsymbol{\xi}_i f_i+(\delta t/2)\mathbf{F_L}$.

C. LB scheme for magnetic field

The next task is to formulate a lattice kinetic equation for the magnetic induction. Since it is not possible to develop a kinetic formulation for the induction equation using a scalar distribution function [10], a vector distribution function (VDF) $\mathbf{g}(\mathbf{x},\boldsymbol{\Xi},t)$ is introduced for monitoring the macroscopic magnetic field. This distribution function may be used in a lattice different from that used for the hydrodynamic DDF [10]. The evolution of $\mathbf{g}$ obeys a vector kinetic equation of the form:

$$\partial_t\mathbf{g}+\boldsymbol{\Xi}\cdot\nabla\mathbf{g}=-(1/\lambda_g)(\mathbf{g}-\mathbf{g}^{eq}), \tag{6}$$

where $\boldsymbol{\Xi}$ corresponds to the particle velocity vector (not necessarily the same as $\boldsymbol{\xi}$), λ_g is the relaxation time, and $\mathbf{g}^{eq}$ is the local EDF. A trapezoidal rule [13] is applied subsequently to obtain the discrete form of the evolution equation

$$\begin{aligned}\mathbf{g}_j(\mathbf{x}+\boldsymbol{\Xi}_j\delta t,\boldsymbol{\Xi}_j,t+\delta t)-\mathbf{g}_j(\mathbf{x},\boldsymbol{\Xi}_j,t)&\\ =-\frac{\delta t}{2\lambda_g}[\mathbf{g}_j(\mathbf{x}+\boldsymbol{\Xi}_j\delta t,\boldsymbol{\zeta}_j,t+\delta t)-\mathbf{g}_j^{eq}(\mathbf{x}+\boldsymbol{\Xi}_j\delta t,\boldsymbol{\Xi}_j,t+\delta t)]&\\ -\frac{\delta t}{2\lambda_g}[\mathbf{g}_j(\mathbf{x},\boldsymbol{\Xi}_j,t)-\mathbf{g}_j^{eq}(\mathbf{x},\boldsymbol{\Xi}_j,t)],&\end{aligned} \tag{7}$$

where $\mathbf{g}_j(\mathbf{x},\boldsymbol{\Xi}_j,t)$ $(j\in\{0,M\})$ is the discrete VDF with the index j stands for the M base vectors of the lattice used for magnetic field calculation. The discrete EDF takes the form $g_{j\beta}^{eq}=W_j[B_\beta+\frac{\Xi_{j\alpha}}{c_g^2}(u_\alpha B_\beta-B_\alpha u_\beta)]$ with α, β denoting the spatial directions and $\alpha\neq\beta$. $\boldsymbol{\Xi}_j$ and W_j are the discrete velocity vectors and the weights of a symmetric lattice satisfying $\Sigma_{j=0}^{M}W_j=1$ and $\Sigma_{j=0}^{M}W_j\Xi_{j\alpha}\Xi_{j\beta}=c_g^2\delta_{\alpha\beta}$. Furthermore, the symmetry of the lattice must ensure $\Sigma_{j=0}^{M}W_j\Xi_{j\alpha}=0$ and $\Sigma_{j=0}^{M}W_j\Xi_{j\alpha}\Xi_{j\beta}\Xi_{j\gamma}=0$. By applying the Chapman-Enskog multiple scale expansion along with the solvability conditions $\Sigma_{j=0}^{M}\mathbf{g}_j^{(n)}=0$ for $n=1,2,\ldots$, the macroscopic magnetic induction equation [Eq. (2)] can be recovered from Eq. (7) provided $\eta=c_g^2(\lambda_g-0.5)\delta t$. Hence the magnetic resistivity may be adjusted independently of the kinematic viscosity. Since the fourth order symmetry is not required in deriving the induction equation, we may use a lattice with less symmetry than the nine-speed lattice used for hydrodynamics. We choose a 5-bit lattice configuration (refer to Fig. 1) in 2D (D2Q5) $(M=4)$ for the magnetic field [10]. The corresponding weights are $W_0=1/3$ and $W_j=1/6$ for $j=1-4$ and $c_g=\varphi/\sqrt{3}$ (same as 9-bit lattice). The macroscopic magnetic field vector can be obtained as $\mathbf{B}=\Sigma_{j=0}^{M}\mathbf{g}_j$.

D. Thermal LB scheme

A relatively stable thermal LB model for the nonisothermal MHD flow can now be constructed from a passive scalar kinetic equation following He *et al.* [13] through the space and time evolution of a separate temperature distribution function (TDF) $h(\mathbf{x},\boldsymbol{\xi},t)$ as:

$$\partial_t h+\boldsymbol{\xi}\cdot\nabla h=-(1/\lambda_h)(h-h^{eq})+\Re+Q, \tag{8}$$

where λ_h is the relaxation time, h^{eq} is the local EDF, $\Re=\Re^I+\Re^{II}+\Re^{III}$, with $\Re^I=-f(\boldsymbol{\xi}-\mathbf{u})\cdot[\partial_t\mathbf{u}+(\mathbf{u}\cdot\nabla)\mathbf{u}]/R$, $\Re^{II}=-f^{eq}[(\boldsymbol{\xi}-\mathbf{u})(\boldsymbol{\xi}-\mathbf{u}):\nabla\mathbf{u}]/R$, and $\Re^{III}=-(f-f^{eq})[(\boldsymbol{\xi}-\mathbf{u})(\boldsymbol{\xi}-\mathbf{u}):\nabla\mathbf{u}]/R$ being respectively associated with the kinetic energy, compression work and viscous heat dissipation [15]. In the incompressible limit $(\mathrm{Ma}\to0)$, $\Re^I$, and $\Re^{II}$ become negligible. Q in Eq. (8) represents a source term taking into account the effect of the magnetic field. One may obtain the evolution equation of the discrete TDF $h_i(\mathbf{x},\boldsymbol{\xi}_i,t)$ $(i\in\{0,N\})$ by integrating the kinetic equation [Eq. (8)] using a trapezoidal rule [13]

$$\begin{aligned}h_i(\mathbf{x}+\boldsymbol{\xi}_i\delta t,\boldsymbol{\xi}_i,t+\delta t)-h_i(\mathbf{x},\boldsymbol{\xi}_i,t)&\\ =-\frac{\delta t}{2\lambda_h}[h_i(\mathbf{x}+\boldsymbol{\xi}_i\delta t,\boldsymbol{\xi}_i,t+\delta t)-h_i^{eq}(\mathbf{x}+\boldsymbol{\xi}_i\delta t,\boldsymbol{\xi}_i,t+\delta t)]&\\ -\frac{\delta t}{2\lambda_h}[h_i(\mathbf{x},\boldsymbol{\xi}_i,t)-h_i^{eq}(\mathbf{x},\boldsymbol{\xi}_i,t)]&\\ +\frac{\delta t}{2}\Re_i(\mathbf{x}+\boldsymbol{\xi}_i\delta t,\boldsymbol{\xi}_i,t+\delta t)+\frac{\delta t}{2}\Re_i(\mathbf{x},\boldsymbol{\xi}_i,t)&\\ +\frac{\delta t}{2}Q_i(\mathbf{x}+\boldsymbol{\xi}_i\delta t,\boldsymbol{\xi}_i,t+\delta t)+\frac{\delta t}{2}Q_i(\mathbf{x},\boldsymbol{\xi}_i,t).&\end{aligned} \tag{9}$$

The discrete EDF takes the form $h_i^{eq}=w_i\rho c_pT[1+\frac{(\boldsymbol{\xi}_i\cdot\mathbf{u})}{c_s^2}+\frac{\mathbf{uu}:(\boldsymbol{\xi}_i\boldsymbol{\xi}_i-c_s^2\mathbf{I})}{2c_s^4}]=c_pTf_i^{eq}$ and $\Re_i=\Re_i^{III}=-T(f_i-f_i^{eq})[(\boldsymbol{\xi}_i-\mathbf{u})(\boldsymbol{\xi}_i-\mathbf{u}):\nabla\mathbf{u}]/c_s^2$, $Q_i=w_iq[1+\frac{(\boldsymbol{\xi}_i\cdot\mathbf{u})}{c_s^2}]+w_ic_pT\frac{\boldsymbol{\xi}_i\cdot\mathbf{F_L}}{c_s^2}$. The two terms appearing in the expression of Q_i represent, respectively, the effects due to Joule heating and electromagnetic force field. The second term specifically implies that the evolution of the TDF is affected by the applied electromagnetic field not only through the Joule heating term but also through the force field [16]. In some limiting case where the Joule heating term is negligibly small, the influence of the source term Q_i still exists. Clearly, Q_i satisfies the properties: $\Sigma_{i=0}^{N}Q_i=q$ and $\Sigma_{i=0}^{N}\boldsymbol{\xi}_iQ_i=\mathbf{u}q+c_pT\mathbf{F_L}$. By invoking the Chapman-Enskog procedure along with these properties, it is possible to recover the macroscopic energy conservation equation [Eq. (3)] from Eq. (9) by setting the thermal diffusivity as $\alpha=\kappa_t/\rho c_p=c_s^2(\lambda_g-0.5)\delta t$. Hence, the thermal diffusivity can now be adjusted independently of the kinematic viscosity and the model becomes suitable for varying Prandtl

number flows. The thermal model is implemented in the same lattice (D2Q9) used for the flow field calculation. The macroscopic temperature can be computed as $\rho c_p T=\Sigma_{i=0}^{N} h_i+(\delta t/2)\Sigma_{i=0}^{N}(\Re_i+Q_i)$.

E. Macroscopic quantities

In order to avoid implicitness of Eqs. (5), (7), and (9), we further introduce:

$$\bar{f}_i = f_i + \frac{\delta t}{2\lambda_f}[f_i - f_i^{eq}] - \frac{\delta t}{2}F_i,$$

$$\bar{\mathbf{g}}_j = \mathbf{g}_j + \frac{\delta t}{2\lambda_g}[\mathbf{g}_j - \mathbf{g}_j^{eq}],$$

and

$$\bar{h}_i = h_i + \frac{\delta t}{2\lambda_h}[h_i - h_i^{eq}] - \frac{\delta t}{2}(\Re_i + Q_i).$$

Consequently, the discretized evolution equations for $\bar{f}_i$, $\bar{\mathbf{g}}_j$ and $\bar{h}_i$ becomes

$$\bar{f}_i(\mathbf{x}+\boldsymbol{\xi}_i\delta t,\boldsymbol{\xi}_i,t+\delta t) = \bar{f}_i(\mathbf{x},\boldsymbol{\xi}_i,t) - \frac{\delta t}{(\lambda_f+0.5\delta t)}[\bar{f}_i(\mathbf{x},\boldsymbol{\xi}_i,t) - f_i^{eq}(\mathbf{x},\boldsymbol{\xi}_i,t)] + \frac{\lambda_f\delta t}{(\lambda_f+0.5\delta t)}F_i(\mathbf{x},\boldsymbol{\xi}_i,t), \tag{10}$$

$$\bar{\mathbf{g}}_j(\mathbf{x}+\boldsymbol{\Xi}_j\delta t,\boldsymbol{\Xi}_j,t+\delta t) = \bar{\mathbf{g}}_j(\mathbf{x},\boldsymbol{\Xi}_j,t) - \frac{\delta t}{(\lambda_g+0.5\delta t)}[\bar{\mathbf{g}}_j(\mathbf{x},\boldsymbol{\Xi}_j,t) - \mathbf{g}_j^{eq}(\mathbf{x},\boldsymbol{\Xi}_j,t)], \tag{11}$$

$$\bar{h}_i(\mathbf{x}+\boldsymbol{\xi}_i\delta t,\boldsymbol{\xi}_i,t+\delta t) = \bar{h}_i(\mathbf{x},\boldsymbol{\xi}_i,t) - \frac{\delta t}{(\lambda_h+0.5\delta t)}[\bar{h}_i(\mathbf{x},\boldsymbol{\xi}_i,t) - h_i^{eq}(\mathbf{x},\boldsymbol{\xi}_i,t)] + \frac{\lambda_h\delta t}{(\lambda_h+0.5\delta t)}[\Re_i(\mathbf{x},\boldsymbol{\xi}_i,t) + Q_i(\mathbf{x},\boldsymbol{\xi}_i,t)]. \tag{12}$$

The macroscopic quantities are now obtained from $\bar{f}_i$, $\bar{\mathbf{g}}_j$, and $\bar{h}_i$ as, $\rho=\Sigma_{i=0}^{N}\bar{f}_i$, $\rho\mathbf{u}=\Sigma_{i=0}^{N}\boldsymbol{\xi}_i\bar{f}_i+(\delta t/2)\mathbf{F_L}$, $\mathbf{b}=\Sigma_{j=0}^{M}\bar{\mathbf{g}}_j$, and $\rho c_p T=\Sigma_{i=0}^{N}\bar{h}_i+(\delta t/2)\Sigma_{i=0}^{N}(\Re_i+Q_i)$. The current density can be computed from the moment of $\bar{\mathbf{g}}$ [10] as:

$$J_\gamma = \frac{1}{\mu}(\nabla\times\mathbf{B})_\gamma = -\frac{1}{c_g^2\lambda_g\mu}\varepsilon_{\alpha\beta\gamma}\left[\sum_{j=0}^{M}\Xi_{j\alpha}\bar{g}_{j\beta} - (u_\alpha B_\beta - B_\alpha u_\beta)\right], \tag{13}$$

where $\varepsilon_{\alpha\beta\gamma}$ is the alternating Levi-Civita tensor.

III. SIMULATION RESULTS

We simulate a thermohydrodynamically fully developed Hartmann flow in a rectangular channel. The Hartmann flow is a classical benchmark MHD problem, which is essentially a stationary flow of an incompressible conductive fluid between two parallel plates subjected to a uniform transverse magnetic field. The two plates are located at $y=+L$ and $y=-L$. The fluid and the plates are kept initially at the same temperature T_0 and a uniform magnetic field of flux density $b_0\hat{\mathbf{e}}_\mathbf{y}$ is applied perpendicular to the plates. The plates are assumed electrically insulating and the thickness of the plates is infinitesimally small such that any temperature variation within the plate itself can be neglected. The flow is considered to be along the x direction with only one component of velocity $\mathbf{u}=u_x\hat{\mathbf{e}}_x$. The flow induces an additional magnetic field of flux density $b_x\hat{\mathbf{e}}_x$ having only a x component. Consequently, the total magnetic field becomes $\mathbf{b}=b_x\hat{\mathbf{e}}_x+b_0\hat{\mathbf{e}}_\mathbf{y}$. From the divergence free conditions along with the fully stabilized flow consideration we obtain $\partial u_x/\partial x=0$, $\partial b_x/\partial x=0$, and $\partial T/\partial x=0$. Consequently the nonlinear terms of the Navier-Stokes, magnetic induction and energy equations vanish. Further, neglecting the kinetic energy and compression work and considering that all variables depend only on y we obtain the simplified governing equations in an incompressible limit as [8,10,17]:

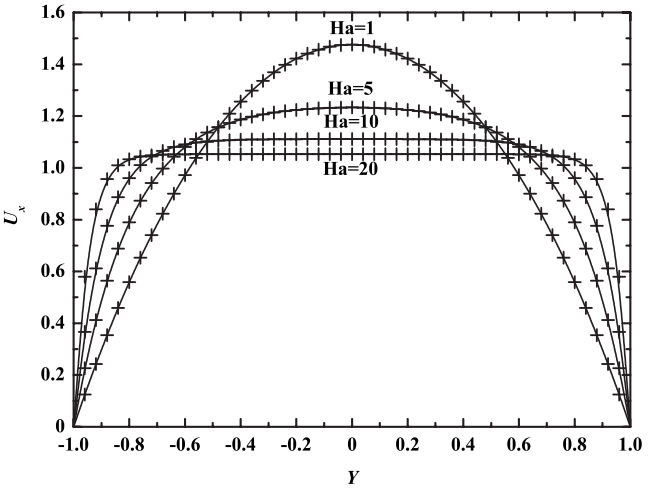

FIG. 2. Dimensionless velocity profiles for different Hartmann numbers. Comparison between analytical (solid lines) and LB (+) results.

$$\frac{1}{\rho}\frac{dp}{dx} = \nu\frac{d^2u_x}{dy^2} + \frac{b_0}{\rho\mu}\frac{db_x}{dy} \tag{14}$$

$$b_0\frac{du_x}{dy} + \eta\frac{d^2b_x}{dy^2} = 0 \tag{15}$$

$$\kappa_t\frac{d^2T}{dy^2} + \rho\nu\left(\frac{du_x}{dy}\right)^2 + \frac{1}{\kappa_e\mu^2}\left(\frac{db_x}{dy}\right)^2 = 0. \tag{16}$$

Equations (14)–(16), subjected to the boundary conditions $u_x(\pm L)=b_x(\pm L)=0$ and $T(\pm L)=T_0$, can be solved analytically [17] to obtain:

$$U_x(Y) = \frac{\mathrm{Ha}[\cosh\mathrm{Ha} - \cosh(\mathrm{Ha}Y)]}{\mathrm{Ha}\cosh\mathrm{Ha} - \sinh\mathrm{Ha}}, \tag{17}$$

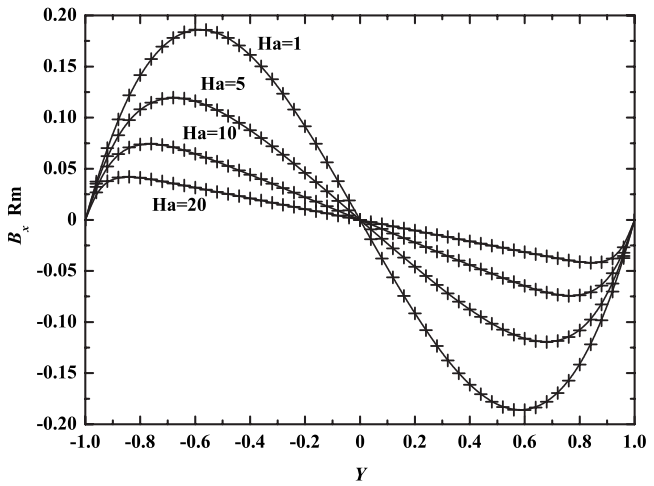

FIG. 3. Dimensionless induced magnetic fields for different Hartmann numbers. Comparison between analytical (solid lines) and LB (+) results.

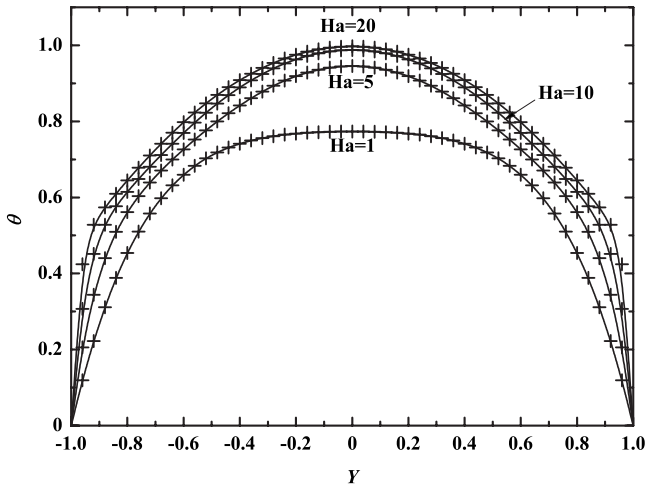

FIG. 4. Dimensionless temperature profiles for different Hartmann numbers. Comparison between analytical (solid lines) and LB (+) results.

$$B_x(Y) = \frac{\mathrm{Rm}\sinh \mathrm{Ha}}{\mathrm{Ha}\cosh \mathrm{Ha} - \sinh \mathrm{Ha}}\left[\frac{\mathrm{Ha}\cosh(\mathrm{Ha}Y)}{\sinh \mathrm{Ha}} - Y\right], \tag{18}$$

$$\Theta(Y) = \frac{\mathrm{Ha}^2}{(\mathrm{Ha}\cosh \mathrm{Ha} - \sinh \mathrm{Ha})^2}\left[\frac{1-Y^2}{2}\sinh^2 \mathrm{Ha} + \frac{\cosh 2\mathrm{Ha} - \cosh 2\mathrm{Ha}Y}{4} - \frac{2\sinh \mathrm{Ha}(\cosh \mathrm{Ha} - \cosh \mathrm{Ha}Y)}{\mathrm{Ha}}\right], \tag{19}$$

where $X=x/L$, $Y=y/L$, $P=p/\rho u_s^2$, $U_x=u_x/u_s$, $B_x=b_x/b_0$, $\Theta=\kappa_t(T-T_0)/\rho\nu u_s^2$, Hartmann number $\mathrm{Ha}=b_0L\sqrt{\kappa_e/\rho\nu}$, kinetic Reynolds number $\mathrm{Re}=u_sL/\nu$, magnetic Reynolds number $\mathrm{Rm}=u_sL/\eta$ with $u_s=\frac{1}{2L}\int_{-L}^{L}u_x(y)dy$ as the characteristic velocity.

Simulation starts from an initial equilibrium state with constant density $\rho=1$ and uniform magnetic field b_0 in the y direction. The normalized velocity, temperature and the horizontal induced magnetic fields are set to zero initially throughout the entire computational domain. It should be mentioned here that the present kinetic scheme for magnetic induction preserves a consistent discrete approximation to $\nabla\cdot\mathbf{B}=0$ to machine round-off error [10]. To drive the flow a small pressure gradient is imposed along x direction. For all simulations an array of 400×50 cells are used and the simulations are carried out until a dynamic steady state is reached. The nonequilibrium extrapolation method [18], which has a good numerical accuracy and stability, is adopted to implement the boundary conditions. The central difference scheme is adopted to discretize the term $\mathfrak{R}_i$. In the present study, we explored values of relaxation parameters $\lambda_f,\lambda_g,\lambda_h>0.5$, which are necessary for the stability of the numerical scheme [19].

Simulation results are obtained for Ha=1, 5, 10, and 20. The Hartmann number is varied by changing the magnitude of the uniform magnetic flux density b_0. Figure 2 depicts the streamwise dimensionless velocity profiles for different Hartmann numbers. It is observed that the relatively flatter velocity profiles at somewhat higher values of Ha tend to become parabolic in nature, as Ha gradually decreases due to the well-known Hartmann effect. The normalized horizontal induced magnetic fields for various Hartmann numbers are shown in Figs. 3 and 4 represents the dimensionless temperature. The temperature is found to increase as usual with increasing Hartmann numbers due to increased Joule heating. The corresponding analytical results are shown simultaneously in the figures and an excellent agreement with the numerical simulation is observed. Similar trends for the velocity and magnetic fields have also been found in [10]. However, the present model differs with the existing isothermal LB MHD models [2–10] in the sense that it is capable of capturing the temperature field driven by the viscous and Joule heating through a passive scalar formulation in the LB framework.

IV. SUMMARY

A LB model for simulating nonisothermal transport phenomena encountered in classical MHD flows in 2D is presented in this article. The model uses three separate distribution functions and relaxation time ($\lambda_f\neq\lambda_g\neq\lambda_h$) to monitor the associated hydrodynamics, magnetodynamics and thermodynamics. Accordingly, it offers better flexibility to independently control the fluid viscosity, magnetic resistivity and thermal diffusivity. Additionally, the model satisfies the divergence free constraint of the magnetic field and it can be extended to 3D in a straightforward manner. The results for the classical Hartmann flow show excellent agreement with the corresponding analytical solution. This suggests that the proposed model can be considered as a starting point for simulating more complex nonisothermal MHD flows in the LB framework.

[1] S. Chen and G. D. Doolen, Annu. Rev. Fluid Mech. **30**, 329 (1998).
[2] H. Chen, W. H. Matthaeus, and L. W. Klein, Phys. Fluids **31**, 1439 (1988).
[3] S. Chen, H. Chen, D. Martinez, and W. Matthaeus, Phys. Rev. Lett. **67**, 3776 (1991).
[4] S. Succi, M. Vergassola, and R. Benzi, Phys. Rev. A **43**, 4521 (1991).
[5] D. O. Martinez, S. Chen, and W. H. Matthaeus, Phys. Plasmas **1**, 1850 (1994).
[6] P. Pavlo, G. Vahala, L. Vahala, and M. Soe, J. Comput. Phys. **139**, 79 (1998).
[7] M. Hirabayashi, Y. Chen, and H. Ohashi, Phys. Rev. Lett. **87**, 178301 (2001).
[8] W. Schaffenberger and A. Hanslmeier, Phys. Rev. E **66**, 046702 (2002).
[9] A. Macnab, G. Vahala, L. Vahala, P. Pavlo, and M. Soe, Czech. J. Phys. **52**, Suppl. D, D59 (2002).
[10] P. J. Dellar, J. Comput. Phys. **179**, 95 (2002).
[11] G. Breyiannis, and D. Valougeorgis, Phys. Rev. E **69**, 065702(R) (2004).
[12] X.-D. Niu, H. Yamaguchi, and K. Yoshikawa, Phys. Rev. E **79**, 046713 (2009).
[13] X. He, S. Chen, and G. D. Doolen, J. Comput. Phys. **146**, 282 (1998).
[14] P. J. Dellar, Phys. Rev. E **64**, 031203 (2001).
[15] Y. Shi, T. S. Zhao, and Z. L. Guo, Phys. Rev. E **70**, 066310 (2004).
[16] Z. Guo, T. S. Zhao, and Y. Shi, J. Chem. Phys. **122**, 144907 (2005).
[17] E. Blums, Yu. Mikhailov, and R. Ozols, *Heat and Mass Transfer in MHD Flows* (World Scientific, Singapore, 1987).
[18] Z. Guo, C. Zheng, and B. Shi, Phys. Fluids **14**, 2007 (2002).
[19] F. J. Higuera, S. Succi, and R. Benzi, EPL **9**, 345 (1989).